*J. Fluid Mech.* (2016), *vol.* 798, *pp.* 682–695. © Cambridge University Press 2016
doi:10.1017/jfm.2016.341



# Forcing-dependent dynamics and emergence of helicity in rotating turbulence

**Vassilios Dallas**[1,†] **and Steven M. Tobias**[1]

[1]Department of Applied Mathematics, University of Leeds, Leeds LS2 9JT, UK

(Received 17 January 2016; revised 4 April 2016; accepted 12 May 2016;
first published online 8 June 2016)

The effects of large-scale mechanical forcing on the dynamics of rotating turbulent flows are studied by means of direct numerical simulations, systematically varying the nature of the mechanical force in time. We find that the statistically stationary solutions of these flows depend on the nature of the forcing mechanism. Rapidly enough rotating flows with a forcing that has a persistent direction relative to the axis of rotation bifurcate from a non-helical state to a helical state despite the fact that the forcing is non-helical. We demonstrate that the nature of the mechanical force in time and the emergence of helicity have direct implications for the cascade dynamics of these flows, determining the anisotropy in the flow, the energy condensation at large scales and the power-law energy spectra that are consistent with previous findings and phenomenologies under strong and weak turbulence.

**Key words:** rotating turbulence, turbulent flows

## 1. Introduction

The effects of the Coriolis force on a turbulent fluid flow become important at sufficiently high rotation rates, altering its dynamics (Tritton 1988). Experiments and simulations reveal that fast rotation renders the flow quasi-two-dimensional (quasi-2D), since fast rotation suppresses the velocity gradients along the axis of rotation as shown by the Taylor–Proudman theorem (Proudman 1916; Taylor 1917). Under such conditions, the flow sustains inertial waves that have a frequency proportional to the rotation rate (Lighthill 1965; Greenspan 1968).

The interplay between inertial waves and eddies in rotating fluids makes the problem of rotating turbulence very rich. Many experimental studies over a wide range of parameters have elucidated the dynamics of such flows (Hopfinger & Heijst 1993; Ruppert-Felsot *et al.* 2005; Davidson, Staplehurst & Dalziel 2006; Bewley *et al.* 2007; van Bokhoven *et al.* 2009; Moisy *et al.* 2011). Many numerical studies have also been carried out on rotating turbulence. The need for a regime that features both fully developed turbulence (large Reynolds number) and fast-rotating flow (small Rossby number) puts strong restrictions on the scale separation requirements in simulations. Therefore, most of the early numerical investigations were focused on decaying rotating turbulence (Bartello, Métais & Lesieur 1994; Hossain 1994; Cambon, Mansour & Godeferd 1997; Morinishi, Nakabayashi & Ren 2001; Teitelbaum &

†Email address for correspondence: v.dallas@leeds.ac.uk

Mininni 2011; Yoshimatsu, Midorikawa & Kaneda 2011). More recent studies have been performed on forced rotating turbulence both at large (Yeung & Zhou 1998; Mininni & Pouquet 2010; Mininni, Rosenberg & Pouquet 2012) and small scales, the latter to study the dynamics of the inverse cascade (Smith, Chasnov & Waleffe 1996; Pouquet *et al.* 2013; Deusebio *et al.* 2014). The computational costs generally prevent the exhaustive coverage of the parameter space, with most numerical studies reaching either large Reynolds numbers and moderate Rossby numbers or moderate Reynolds numbers and small Rossby numbers. Note that these simulations, with the exception of a very recent study which reached steady states and extensively covered a fairly large portion of the parameter space (Alexakis 2015), have not reached statistically stationary solutions because very long integration times are required.

Although these studies are numerous and an adequate portion of the parameter space has been covered, there are still disparate results in different cases – for example, different power-law spectra with $E(k) \propto k^{-5/3}$, $k^{-2}$ and $k^{-5/2}$, supported theoretically by strong and weak-wave turbulence phenomenologies (Kolmogorov 1941; Zhou 1995; Galtier 2003; Pouquet & Mininni 2010). Moreover, a recent investigation has shown sensitivity to forcing, in that different results were found for the large scales of a flow that was forced at intermediate scales (Sen *et al.* 2012) when energy was injected exclusively into the quasi-2D component of the flow, compared with when it was injected solely into the inertial waves. The injection of helicity into the flow has also shown alterations in the behaviour of the cascade (Pouquet & Mininni 2010). Forcing-dependent dynamics have been observed in various other systems such as in 2D turbulence (Bracco & McWilliams 2010; Boffetta & Ecke 2012), in beta-plane turbulence (Maltrud & Vallis 1991) and in magnetohydrodynamic turbulence (Dallas & Alexakis 2015).

The present work focuses on the effects of the mechanical force on the dynamics of rotating flows by means of numerical simulations, varying systematically the memory time scale of the mechanical force (i.e. the time scale on which the phases of the force are randomised). The behaviour of different mechanical forcing mechanisms on the flows is also considered for different rotation rates. To the best of the authors' knowledge this is the first study of forced rotating flows in the steady-state regime in which the effects of a large-scale external force on the dynamics are studied extensively.

The paper is structured as follows. All the necessary details of the formulation of our direct numerical simulation (DNS) of forced rotating turbulence are provided in § 2. Section 3 analyses the dynamics of the flows with different memory time scales of the forcing mechanism for a given Rossby number. Here, we also focus on the spontaneous emergence of helicity in our flows and its influence on the anisotropy and spectral dynamics. In § 4 we describe the Rossby number dependence on flows with different types of forcing mechanisms and we justify the spontaneous mirror-symmetry breaking in our flows even though net helicity is not injected directly. Finally, in § 5, we conclude by summarising our findings and discussing the implications of our work.

## 2. Numerical simulations

In this study, we consider the three-dimensional (3D) incompressible Navier–Stokes equations in a rotating frame of reference

$$\partial_t \boldsymbol{u} + \boldsymbol{\omega} \times \boldsymbol{u} + 2\boldsymbol{\Omega} \times \boldsymbol{u} = -\boldsymbol{\nabla} P + \nu \nabla^2 \boldsymbol{u} + \boldsymbol{f}, \tag{2.1}$$

where $\boldsymbol{u}$ is the velocity field, $\boldsymbol{\omega} = \boldsymbol{\nabla} \times \boldsymbol{u}$ is the vorticity, $P$ is the pressure, $\nu$ is the kinematic viscosity and $\boldsymbol{f}$ is an external mechanical force. In a Cartesian domain,

we choose the rotation axis to be in the $z$ direction with $\boldsymbol{\Omega} = \Omega \boldsymbol{e}_z$, where $\Omega$ is the rotation frequency. In the ideal case of $\nu = 0$ and $\boldsymbol{f} = 0$, equation (2.1) conserves the energy $E = \langle |\boldsymbol{u}|^2 \rangle / 2$ (where $|\cdot|$ stands for the $L_2$-norm) and the helicity $H = \langle \boldsymbol{u} \cdot \boldsymbol{\omega} \rangle$ with the angular brackets denoting a spatial average unless indicated otherwise.

The external mechanical forcing in (2.1) is given by

$$\boldsymbol{f} = f_0 \sum_{k_f} \begin{pmatrix} \sin(k_f y + \phi_y) + \sin(k_f z + \phi_z) \\ \sin(k_f x + \phi_x) + \sin(k_f z + \phi_z) \\ \sin(k_f x + \phi_x) + \sin(k_f y + \phi_y) \end{pmatrix}, \tag{2.2}$$

where $\phi_x$, $\phi_y$, $\phi_z$ are phases, randomised every $\tau_m$, of the so-called memory time scale, which is one of the control parameters in our study. The forcing is applied at wavenumber amplitudes $|\boldsymbol{k}| = k_f = 2$, 3 and 4, where $k_f$ denotes the forcing wavenumber. The random phases are specific to a $k_f$ mode and the random change of phases is done instantaneously for all phases. In the limit of $\tau_m \to 0$ we have essentially a random delta correlated in time forcing with the phases randomised at each time step, whereas when we choose $\tau_m = \infty$ we randomise the phases only at $t = 0$ in the duration of the runs, and hence apply a time-independent forcing. For all the runs the forcing amplitude is normalised such that $\boldsymbol{f}/|\boldsymbol{f}| = f_0 = 1$. Note that our forcing mechanism has $\boldsymbol{f} \cdot \boldsymbol{\nabla} \times \boldsymbol{f} \neq 0$ pointwise in space but it is non-helical on average $\langle \boldsymbol{f} \cdot \boldsymbol{\nabla} \times \boldsymbol{f} \rangle = 0$, unlike an ABC forcing (Dombre *et al.* 1986) which is fully helical.

Now, if we write the wavenumbers in the 3D Fourier space using cylindrical coordinates, we have $\boldsymbol{k} = (\boldsymbol{k}_\perp, \boldsymbol{k}_\parallel)$, with $k_\perp = \sqrt{k_x^2 + k_y^2}$ and $k_\parallel = |k_z|$. Then, the 2D modes (i.e. independent of $z$) in Fourier space can be denoted as $\boldsymbol{u}(\boldsymbol{k}_\perp)$ and the 3D or wave modes as $\boldsymbol{u}(\boldsymbol{k})$. Then, in this setting the time-independent forcing ($\tau_m = \infty$) excites two 2D modes (in the $k_x$ and $k_y$ axis of the Fourier space) and one 3D mode (in the $k_z$ axis) in the Fourier shell for each wavenumber $k_f$. The random-in-time forcing ($\tau_m \to 0$) excites also the same modes but since the phases are random, this mechanism is isotropic in contrast to the time-independent forcing. By isotropic, we mean that the forcing vector of the driving mechanism with the short memory time scale samples all phase space assuming ergodicity.

The relevant dimensionless control parameters of our problem are defined based on the forcing amplitude. So, the Reynolds number is given by $Re_f = U/(k_{min}\nu)$ and the Rossby number by $Ro_f = Uk_{min}/(2\Omega)$ where $U = (f_0/k_{min})^{1/2}$. Using these definitions $Re_f^2$ is essentially the Grashof number and $Ro_f$ the ratio of the rotation period $\tau_w \propto \Omega^{-1}$ to the eddy turnover time $\tau_{NL} = (Uk_{min})^{-1}$. Note that $Re_f$ and $Ro_f$ are control parameters in that they do not require knowledge of the solution to be evaluated and are useful for comparison with body-forced numerical simulations or experiments. All the control parameters of our DNS are listed in table 1.

Using the pseudo-spectral method, we numerically integrate (2.1) in a periodic box of size $2\pi$, satisfying the incompressibility condition $\boldsymbol{\nabla} \cdot \boldsymbol{u} = 0$. The time derivatives are estimated using a third-order Runge–Kutta scheme. Aliasing errors are removed using the 2/3 dealiasing rule and as a result the minimum and maximum wavenumbers are $k_{min} = 1$ and $k_{max} = N/3$, respectively, where $N$ is the number of grid points in each Cartesian coordinate. For more details on the numerical code see Gómez, Mininni & Dmitruk (2005).

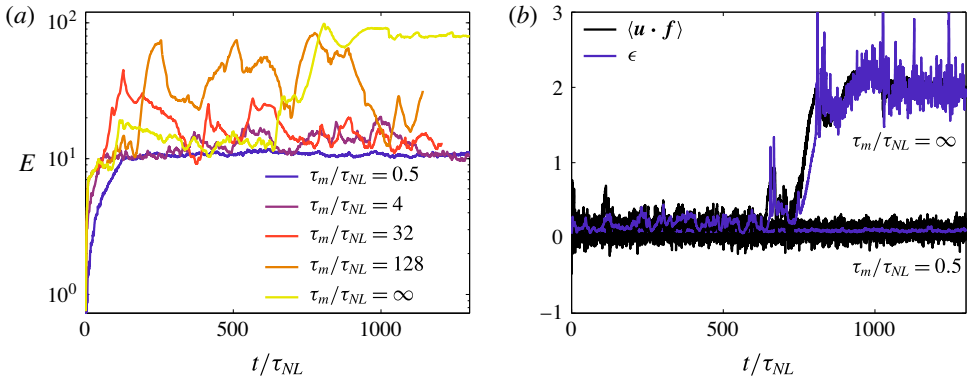


FIGURE 1. (Colour online) Time series of (*a*) the energy $E$ for the flows with different memory time scales $\tau_m$ of the forcing and of (*b*) the rates of energy dissipation $\epsilon$ and injection $\langle \boldsymbol{u} \cdot \boldsymbol{f} \rangle$ for the flows with $\tau_m/\tau_{NL} = 0.5$ and $\infty$ at Rossby number $Ro_f = 0.1$ and Reynolds number $Re_f = 333$.

| $\tau_m/\tau_{NL}$ | 0.5 | 0.5 | 0.5 | 0.5 | 0.5 | 0.5 | 4.0 | 32.0 | 128.0 | $\infty$ | $\infty$ | $\infty$ | $\infty$ | $\infty$ | $\infty$ | $\infty$ |
|---|---|---|---|---|---|---|---|---|---|---|---|---|---|---|---|---|
| $Ro_f$ | 0.01 | 0.05 | 0.1 | 0.1 | 0.2 | 0.5 | 0.1 | 0.1 | 0.1 | 0.01 | 0.05 | 0.1 | 0.1 | 0.2 | 0.33 | 0.5 |
| $Re_f$ | 333 | 333 | 333 | 714 | 333 | 333 | 333 | 333 | 333 | 333 | 333 | 333 | 714 | 333 | 333 | 333 |
| $\Omega$ | 50.0 | 10.0 | 5.0 | 5.0 | 2.5 | 1.0 | 5.0 | 5.0 | 5.0 | 50.0 | 10.0 | 5.0 | 5.0 | 1.0 | 1.5 | 1.0 |
| $\nu$ $(\times 10^{-3})$ | 3.0 | 3.0 | 3.0 | 1.4 | 3.0 | 3.0 | 3.0 | 3.0 | 3.0 | 3.0 | 3.0 | 3.0 | 1.4 | 3.0 | 3.0 | 3.0 |
| $N$ | 256 | 256 | 256 | 512 | 256 | 256 | 256 | 256 | 256 | 256 | 256 | 256 | 512 | 256 | 256 | 256 |

TABLE 1. Numerical control parameters of the DNS.

## 3. Forcing-dependent dynamics

### 3.1. *Time evolution*

Figure 1(*a*) shows the temporal evolution of the energy $E$ for flows with $Ro_f = 0.1$ and different memory time scale $\tau_m$ of the forcing. As $\tau_m$ increases, we observe a gradual increase of the amplitude of the energy up to an order of magnitude. The time-series for $\tau_m/\tau_{NL} > 4$ are characterised by large signal variations, which require extremely long time-integrations, restricting our runs to moderate Reynolds numbers. Note that even for low $\tau_m$ a steady state is reached after a transient that lasts for about 50 to $100\tau_{NL}$ turnover times, indicating how expensive computationally it is to reach a steady-state regime in rotating flows forced at large scales.

The temporal evolution of the energy dissipation rate $\epsilon = \nu\langle|\boldsymbol{\omega}|^2\rangle$ and the energy injection rate $\langle \boldsymbol{u} \cdot \boldsymbol{f} \rangle$ are presented in figure 1(*b*). For clear illustration purposes we choose to plot only the two extreme cases of the flows with highly random-in-time forcing ($\tau_m/\tau_{NL} = 0.5$) and time-independent forcing ($\tau_m/\tau_{NL} = \infty$) at $Ro_f = 0.1$. At relatively early times the two flows reach a steady state (see figure 1*a*) and therefore the balance $\epsilon = \langle \boldsymbol{u} \cdot \boldsymbol{f} \rangle$ is satisfied with both flows having the same rates of energy injection and dissipation. However, after a very long time period ($\sim 600\tau_{NL}$ turnover times) the flow with the time-independent forcing deviates eventually to a new statistically steady state. This happens when $\boldsymbol{u}$ becomes correlated with $\boldsymbol{f}$ and then the flow adjusts its dissipation rate such that a new steady state is achieved.

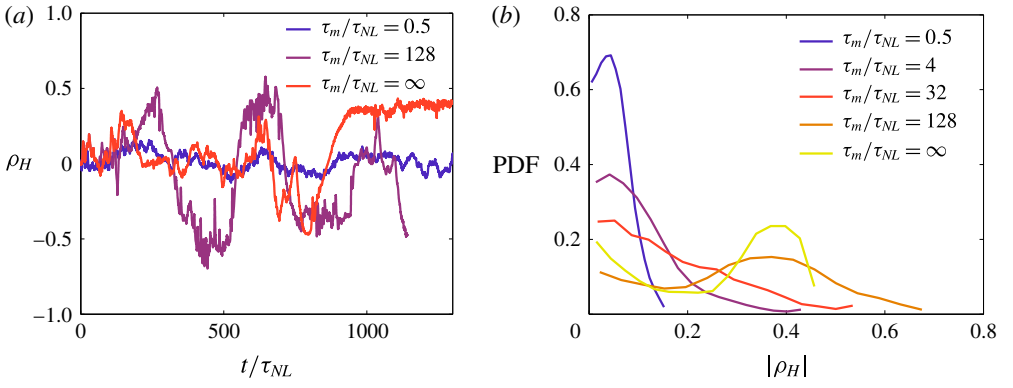


FIGURE 2. (Colour online) (*a*) Time series of relative helicity $\rho_H$ and (*b*) probability density function (PDF) of the absolute value of $\rho_H$ for flows with different forcing memory time scales at Rossby number $Ro_f = 0.1$ and Reynolds number $Re_f = 333$.

The adjustment of the dissipation rate by the flow owing to the increase of the correlation between the external mechanical force and the velocity field explains why the energy increases as we increase the memory time scale of the forcing. This is a very interesting property of rotating flows from a practical point of view if one wants to minimise or maximise the energy dissipation rate in a potential application such as in turbomachinery.

We should point out here that the energy dissipation rate remains small for the flow, with $\tau_m/\tau_{NL} = 0.5$ throughout the duration of the simulation, for two reasons. The first reason is the short memory time scale of the forcing that keeps the $\langle \boldsymbol{u} \cdot \boldsymbol{f} \rangle$ correlation small, and the second reason is the low Rossby number, resulting in a weak turbulent cascade as we show later on.

### 3.2. *The role of helicity*

Helicity is common in real flows and it can be created, for example, in planetary atmospheres in the presence of rotation and stratification (Moffatt 1978; Tobias 2009; Marino *et al.* 2013). In homogenenous non-rotating turbulence it is expected that the helicity spectrum cannot develop if it is initially zero (André & Lesieur 1977) or if an external mechanism does not inject net helicity (Dallas, Fauve & Alexakis 2015). In our runs zero net helicity is injected into the flow. Nevertheless, for a given rotation rate (i.e. $Ro_f = 0.1$) we observe that the relative helicity $\rho_H = H/(|\boldsymbol{u}|\,|\boldsymbol{\omega}|)$ increases as the memory time scale of the forcing increases (see figure 2).

It is apparent from figure 2 that the mirror-symmetry breaking depends on the value of $\tau_m$. Figure 2(*a*) shows $\rho_H$ to be almost zero at early times for all the flows, and as $\tau_m$ increases the mirror symmetry breaks at later times only for long enough $\tau_m$. We observe that helicity emerges in the flow as soon as $\tau_m$ becomes of the order of the eddy turnover time, i.e. $\tau_m/\tau_{NL} \sim O(1)$. To analyse further this behaviour of $\rho_H$ we plot the probability density function (PDF) of the time series of the absolute value of relative helicity in figure 2(*b*). This plot shows an increase in the mean value of $|\rho_H|$ and also a broadening of the tails of the PDFs for longer memory time scales. So, unlike in homogeneous turbulence, helicity can be created in rotating flows by an external force with a sufficiently long memory time scale, even though net helicity is not injected directly into the flow.

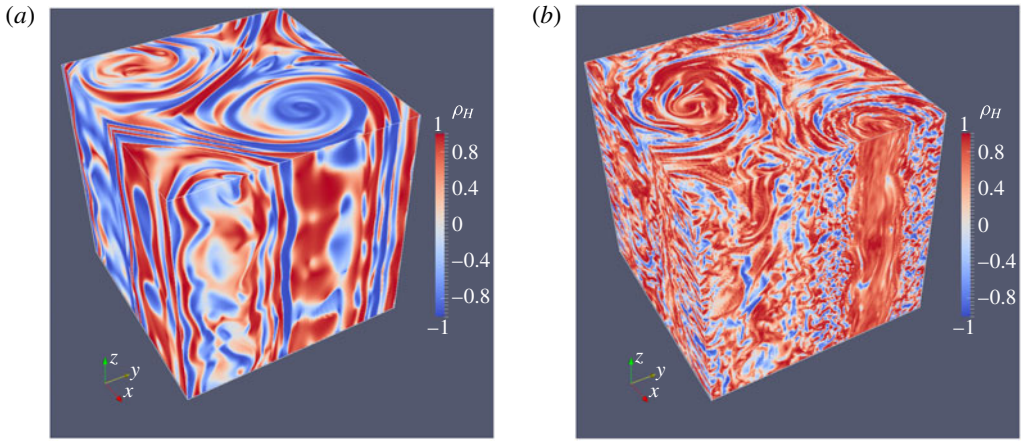


FIGURE 3. (Colour online) Visualisations of the relative helicity $\rho_H$ for the flows at Rossby number $Ro_f = 0.1$ and Reynolds number $Re_f = 714$ with (*a*) $\tau_m/\tau_{NL} = 0.5$, $\rho_H = -0.018$ and (*b*) $\tau_m/\tau_{NL} = \infty$, $\rho_H = 0.45$.

To determine whether the breaking of mirror-symmetry, which distinguishes flows with highly random-in-time and time-independent forcings, remains at higher Reynolds numbers we carried out simulations for the two extreme cases of $\tau_m/\tau_{NL} = 0.5$ and $\infty$ at $Re_f = 714$ and $Ro_f = 0.1$. Our numerical simulations confirmed the persistence of this behaviour at higher Reynolds numbers. We therefore analyse these higher Reynolds number runs in order to gain further insight into the effects of helicity on the flow.

Visualisations of the relative helicity of the flows with $Re_f = 714$ are presented in figures 3(*a*) and 3(*b*) with the average value of $\rho_H = -0.018$ for $\tau_m/\tau_{NL} = 0.5$ and $\rho_H = 0.45$ for $\tau_m/\tau_{NL} = \infty$. The red and blue colours in figure 3 indicate right-hand (positive helicity) and left-hand (negative helicity) circularly polarized helical waves, respectively. An instructive way to explain this further is to decompose the velocity field into circularly polarised helical waves (Constantin & Majda 1988; Waleffe 1992)

$$\boldsymbol{u}(\boldsymbol{x}, t) = \boldsymbol{h}_{\pm}(\boldsymbol{k}) \mathrm{e}^{\mathrm{i}(\boldsymbol{k}\cdot\boldsymbol{x} - \omega_{\pm} t)}, \tag{3.1}$$

where $\mathrm{i}\boldsymbol{k}$, $\boldsymbol{h}_+$ and $\boldsymbol{h}_-$ are the linearly independent eigenvectors of the curl operator, i.e. $\mathrm{i}\boldsymbol{k} \times \boldsymbol{h}_{\pm} = \pm|\boldsymbol{k}|\boldsymbol{h}_{\pm}$. These complex eigenvectors are orthogonal to each other and are fully helical. So, now $\widehat{\boldsymbol{u}}(\boldsymbol{k})$ can be expressed as a linear combination of the eigenvectors $\boldsymbol{h}_+$ and $\boldsymbol{h}_-$ only as follows

$$\widehat{\boldsymbol{u}}(\boldsymbol{k}, t) = u_+(\boldsymbol{k}, t)\boldsymbol{h}_+(\boldsymbol{k}) + u_-(\boldsymbol{k}, t)\boldsymbol{h}_-(\boldsymbol{k}) \tag{3.2}$$

since $\boldsymbol{k} \cdot \widehat{\boldsymbol{u}}(\boldsymbol{k}) = 0$. Then, the helicity can be separated into modes of positive and negative helicity, viz.

$$\begin{aligned} H &= \sum_{\boldsymbol{k}} \widehat{\boldsymbol{u}}(\boldsymbol{k}) \cdot \widehat{\boldsymbol{\omega}}^*(\boldsymbol{k}) \\ &= \sum_{\boldsymbol{k}} k(|u_+(\boldsymbol{k})|^2 - |u_-(\boldsymbol{k})|^2) \\ &= k(E_+ - E_-) = H_+ - H_-, \end{aligned} \tag{3.3}$$

where $^*$ denotes the complex conjugate.

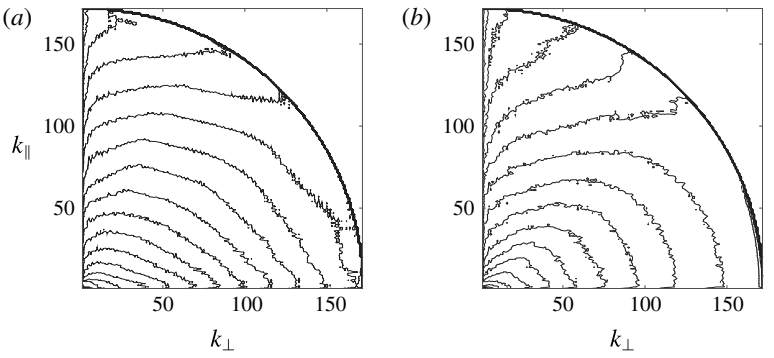


FIGURE 4. The two-dimensional energy spectrum $E_{2D}(k_\perp, k_\parallel)$ for the flows at Rossby number $Ro_f = 0.1$ and Reynolds number $Re_f = 714$ with (*a*) $\tau_m/\tau_{NL} = 0.5$, $\rho_H = -0.018$ and (*b*) $\tau_m/\tau_{NL} = \infty$, $\rho_H = 0.45$.

The nature of the forcing is clearly imprinted on the flow structure in figure 3. The flow with the highly random-in-time forcing (see figure 3*a*) gives a quasi-2D flow with two large columnar vortices, typical at low Rossby numbers due to the Taylor–Proudman theorem. These two vortices are governed by helical waves of opposite polarity. On the other hand, the flow with the time-independent forcing is characterised by helical waves of opposite polarity that travel within the flow, breaking the quasi-2D behaviour at small and intermediate scales that is imposed by rotation (see figure 3*b*). Note that the two large-scale vortices are still present but this time they have the same sign of helicity on average. Similar effects of helicity have also been observed on a previous study of decaying rotating turbulence (Morinishi *et al.* 2001).

In order to quantify the level of anisotropy of these two runs we consider the 2D energy spectrum, which is defined as

$$E_{2D}(k_\perp, k_\parallel) = \sum_{\substack{k_\parallel \leqslant |\boldsymbol{k}\cdot\boldsymbol{e}_z| < k_\parallel + 1 \\ k_\perp \leqslant |\boldsymbol{k}\times\boldsymbol{e}_z| < k_\perp + 1}} |\widehat{\boldsymbol{u}}_{\boldsymbol{k}}|^2. \tag{3.4}$$

The sum is restricted here at energy in cylinders of radius $k_\perp$ and energy in planes $k_\parallel$. Figures 4(*a*) and 4(*b*) show the 2D energy spectrum for the flows with $\tau_m/\tau_{NL} = 0.5$ and $\infty$, respectively. The contours of the 2D energy spectrum for an isotropic flow are represented by concentric circles centred at the origin of the axes. Any deviation from the circular pattern indicates the level of anisotropy in the flow. By comparing the two contour plots of $E_{2D}$, it becomes clear that in figure 4(*b*) the intermediate and small scales are closer to isotropy, implying that the flow with the time-independent forcing is overall less anisotropic than the flow with the highly random-in-time forcing. This observation is in agreement with the visualisation of figure 3, which prompts us to postulate that the helicity plays a central role in the suppression of anisotropy in the flow.

### 3.3. *Spectral behaviour*

In this section we present the spectra of the energy $E(k)$ and the energy flux $\Pi_E(k)$. The energy spectrum was spherically averaged using the following expression:

$$E(k) = \sum_{k \leqslant |\boldsymbol{k}| < k+1} |\widehat{\boldsymbol{u}}_{\boldsymbol{k}}|^2 \tag{3.5}$$

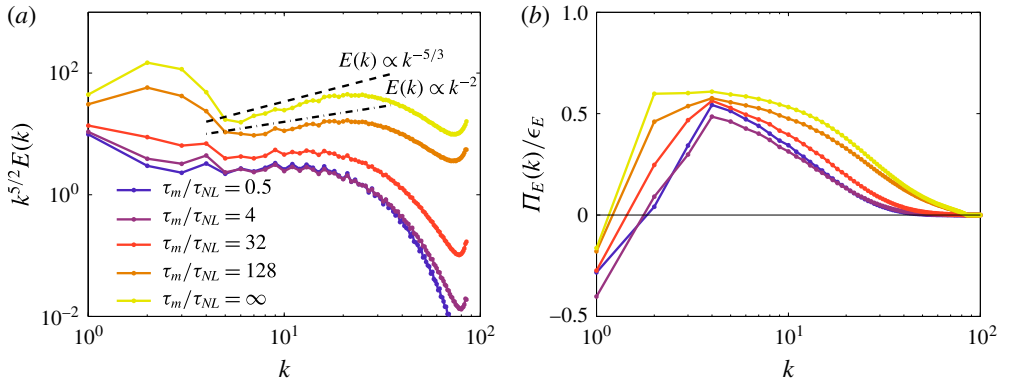


FIGURE 5. (Colour online) (*a*) Energy spectra $E(k)$ compensated by $k^{5/2}$ and (*b*) the energy flux spectra $\Pi_E(k)$ normalised with the dissipation rate $\epsilon_E$ for flows with different forcing memory time scale at Rossby number $Ro_f = 0.1$ and Reynolds number $Re_f = 333$.

and the spectrum of the energy flux was obtained as

$$\Pi_E(k) = \sum_{k=1}^{K} \sum_{k \leqslant |\boldsymbol{k}| < k+1} \widehat{\boldsymbol{u}}^*(\boldsymbol{k}) \cdot \widehat{(\boldsymbol{u} \times \boldsymbol{\omega})}(\boldsymbol{k}). \tag{3.6}$$

The energy flux is a measure that illustrates the direction of the energy cascades. These spectra were time-averaged after the flows had reached a steady-state solution. Note that the flow with the time-independent forcing ($\tau_m/\tau_{NL} = \infty$) was time-averaged only after $\sim 800\tau_{NL}$ turnover times, when the new steady state was reached (see figure 1*b*).

Note that we did not observe any differences to the scalings of the spectra when averaging over spheres and over cylinders. This has also been shown clearly by Mininni, Alexakis & Pouquet (2009), who performed simulations at low Rossby numbers and of similar resolutions to ours. So, the scalings of the spectra that we present are also valid for energy spectra as a function of $k_\perp$. However, significant differences in the scalings are observed in the $k_\parallel$ direction.

The effects of the memory time scale of the forcing are also apparent on the spectral dynamics of our flows. Figure 5(*a*) shows the energy spectra of the flows with different memory time scales of the forcing compensated by $k^{5/2}$. The spectra of these flows obey different power laws which clearly depend on the memory time scale of the forcing. The runs that are forced with the highly random-in-time forcing seem to have a $k^{-5/2}$ scaling. As $\tau_m$ increases the spectra start to deviate gradually from the $k^{-5/2}$ scaling towards a $k^{-2}$ and finally reach a $k^{-5/3}$ scaling for the flow with the time-independent forcing. The $k^{-5/3}$ energy spectrum can be interpreted from the fact that the intermediate and small scales of the flow are closer to isotropy (see figures 4*b* and 3*b*) and hence we expect the Kolmogorov phenomenology to be valid in this case. All the exponents that we observe here could be related to the various phenomenologies on strong and weak-wave turbulence in the literature, where the interplay between $\tau_{NL}$ and the time scale of the inertial waves $\tau_w \propto \Omega^{-1}$ is central to obtain the different energy spectra. These spectral exponents have also been observed in other studies of forced rotating flows (Yeung & Zhou 1998; Mininni & Pouquet 2010; Alexakis 2015). Owing to the moderate resolution of these simulations,

the statements about the exact spectral exponents are qualitative. In any case, our results clearly show a dependence of the spectra on the nature of the forcing in rotating turbulence. Simulations integrated for extremely long times with higher Reynolds numbers but also lower Rossby numbers, falling in the same dynamical regime of the two-dimensional parameter space, are necessary to verify whether our results imply a lack of universality in these flows.

The corresponding spectra for the energy flux $\Pi_E(k)$ normalised by the energy dissipation rate $\epsilon_E = 2\nu \sum_k k^2 E(k)$ are shown in figure 5(*b*). The positive flux in this plot indicates a forward cascade while the negative flux indicates a transfer of energy from the small to the large scales of the flow. In the case of negative flux we do not talk about a cascade because we do not have enough scale separation between the forcing scale and the box size. As the memory time scale of the forcing increases, the forward cascade becomes stronger. On the other hand, the flux of energy towards the large scales increases as the forcing becomes more random-in-time with the flow reaching a quasi-2D state. These observations are in line with the visualisations of figure 3.

We have already seen that as the forcing becomes less time-dependent, helicity increases considerably in our flows, so these changes in the spectra can also be related to the presence of strong net helicity in the flow. This is in agreement with prior studies that have shown the influence of helicity on the energy spectrum by directly injecting helicity into the flow (Mininni & Pouquet 2009, 2010). In contrast, helicity does not seem to have any significant effect on the spectra in non-rotating, homogeneous and isotropic helical turbulence (Dallas *et al.* 2015).

The fact that helicity is not a sign-definite quantity and because we do not inject any net helicity, the sign of helicity in our flows undergoes changes in its inertial range. Therefore, there is either no power-law or it is difficult to define one in our helicity spectra. For this reason, we do not show any helicity spectra here. In the next section, we examine the Rossby number dependence of the dynamics of the flows.

## 4. Rossby number dependence

### 4.1. *Global behaviour*

In the previous sections we saw that the dynamics depend on the nature of the forcing for a given Rossby number. Here, we investigate the effects of the rotation rate on the flows, focusing on the extreme cases of the forcing being highly random-in-time ($\tau_m/\tau_{NL} = 0.5$) and time-independent ($\tau_m/\tau_{NL} = \infty$) for fixed $Re_f = 333$. Again here we restrict ourselves to moderate Reynolds numbers because extremely long integration times for the runs with time-independent forcing are inevitable.

For high Rossby number flows the effect of rotation is negligible and the energy is expected to flow to scales smaller than the forcing scale. However, as the Rossby number is decreased and the flow tends to become quasi-2D, there is more and more energy transferred to scales larger than the forcing scale due to an inverse cascade (Pouquet *et al.* 2013).

We examine the energy and the relative helicity for runs with different Rossby numbers. The triangles and circles denote runs forced with a time-independent forcing and random-in-time forcing, respectively. As the Rossby number is decreased we see that energy increases as expected (see figure 6*a*). However, the rate of increase and the values of energy for high enough rotation rates depend on the nature of the mechanical force. Note that the flow with the time-independent forcing has much more energy at small Rossby numbers.

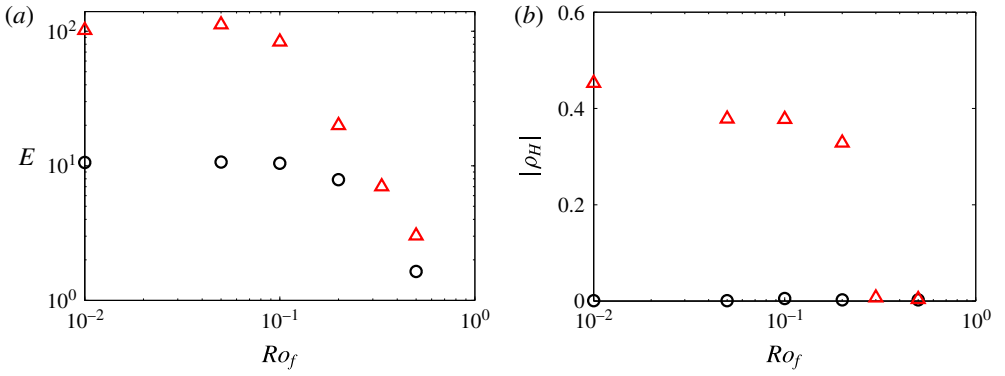


FIGURE 6. (Colour online) Rossby number dependence of (*a*) energy and (*b*) absolute value of relative helicity for flows with Reynolds number $Re_f = 333$. The ○ and △ denote runs forced with $\tau_m/\tau_{NL} = 0.5$ and $\tau_m/\tau_{NL} = \infty$, respectively.

The relative helicity also behaves very differently for the two types of flows and this is shown in figure 6(*b*). The flow with the random-in-time forcing has zero net helicity for all $Ro_f$. However, the flow with the time-independent forcing bifurcates to a state of non-zero helicity for small enough Rossby numbers. The value of $|\rho_H|$ seems to vary discontinuously as $Ro_f$ is decreased with the flow bifurcating to a helical state at the critical $Ro_f^{crit} \simeq 0.2$. Thus, the transition from the non-helical to the helical state is a jump bifurcation. In summary, net helicity emerges in the flow only for small enough $Ro_f$ and long enough $\tau_m$.

Helicity is a pseudoscalar quantity and $H \neq 0$ only if it is directly injected into the flow (i.e. $\boldsymbol{u} \cdot (\boldsymbol{\nabla} \times \boldsymbol{f}) \neq 0$) by a helical mechanical force or if another pseudoscalar quantity exists related to the pseudovector $\boldsymbol{\nabla} \times \boldsymbol{f}$. In our work, we observe that net helicity emerges in rapidly rotating flows with long enough memory time scale forcings only. So, a pseudovector that relates the rotation vector with the forcing is $\boldsymbol{\Omega} \times (\boldsymbol{\nabla} \times \boldsymbol{f})$ and hence the pseudoscalar quantity that will allow the generation of helicity in a rotating flow is

$$H \propto \boldsymbol{u} \cdot \boldsymbol{\Omega} \times (\boldsymbol{\nabla} \times \boldsymbol{f}). \tag{4.1}$$

A similar expression was derived in a different way by Hide (1975) for a rapidly rotating flow in geostrophic balance assuming that the nonlinear term is negligible. Now, from (4.1) we can deduce that no net helicity will be generated for a short memory time scale forcing since $\langle \boldsymbol{\nabla} \times \boldsymbol{f} \rangle_t = 0$ (with $\langle \cdot \rangle_t$ denoting an average over time), assuming isotropy and ergodicity. On the other hand, for a forcing with long enough memory time scale $\langle \boldsymbol{\nabla} \times \boldsymbol{f} \rangle_t = \boldsymbol{g}(\boldsymbol{x}) \neq 0$ and therefore $H \neq 0$ for long enough integration time scales, in agreement with our observations.

Moffatt (1970) suggested that a random superposition of inertial waves will exhibit a lack of mirror-symmetry if and only if there is a mechanical excitation in a preferred direction in the propagation of the waves with respect to the axis of rotation. Otherwise, the random superposition of inertial waves in equal proportions would give zero net helicity. Based on (4.1), we conjecture that such a mechanism is pertinent to our flows where the angle $\varphi$ between $\Omega \boldsymbol{e}_z$ and $\boldsymbol{\nabla} \times \boldsymbol{f}$ is fixed at time $t = 0$ for a time-independent forcing, and hence such a forcing can add a preferred direction of propagation to the inertial waves, inducing the mirror-symmetry breaking

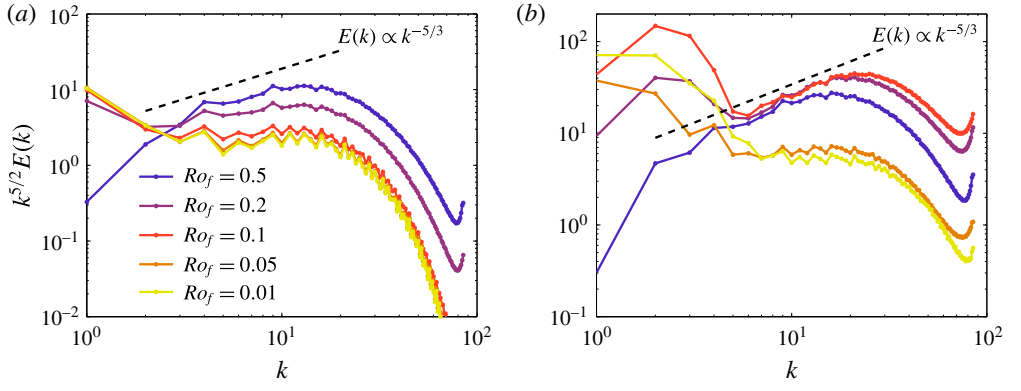


FIGURE 7. (Colour online) Energy spectra $E(k)$ compensated by $k^{5/2}$ for the flows with (*a*) $\tau_m/\tau_{NL} = 0.5$ and (*b*) $\tau_m/\tau_{NL} = \infty$ at different Rossby numbers and Reynolds number $Re_f = 333$.

in our flows. From the other side, a highly random-in-time forcing can excite inertial waves in all directions in equal proportions since $\varphi$ is random in time, and this is why the net helicity remains zero for any value of $Ro_f$ in this case.

### 4.2. *Spectral behaviour*

Here we analyse the energy spectra of the flows at different Rossby numbers. In figure 7(*a*) we present the energy spectra $E(k)$ compensated by $k^{5/2}$ of flows with highly random-in-time forcing. For $Ro_f = 0.5$ the energy spectrum is close to the Kolmogorov $k^{-5/3}$ scaling with the effects of the Coriolis force having no significant influence on the dynamics of the flow. However, as the Rossby number decreases $\tau_w \propto \Omega^{-1}$ becomes the dominant time scale and then the spectrum is changed to the weak-wave turbulence prediction of $E(k) \propto k^{-5/2}$.

Similar behaviour is observed for the spectra of the flows with time-independent forcing (see figure 7*b*) but with two different characteristics. The first is the significant condensation of energy at large scales for small enough Rossby numbers in comparison to the flows with random-in-time forcing. The second is the transition from the Kolmogorov-like regime with $\tau_E \ll \tau_w$ to the weak-wave turbulence regime with $\tau_w \ll \tau_E$ which occurs at lower Rossby numbers, showing the dependence of this transition on the nature of the mechanical force.

Here, we should point out that weak-wave turbulence theory arguments, which assume uniform and isotropic forcing, predict a $k^{-5/2}$ spectrum but they do not predict condensation of energy at large scales due to an inverse cascade in unbounded domains. This is in agreement with figure 7(*a*) where there is some energy condensation at large scales but it is not significant in comparison to figure 7(*b*). However, the energy condensation at large scales in figure 7(*b*) suggests that weak-wave turbulence theory is not necessarily valid for the small Rossby number flows with time-independent forcing even though $E(k) \propto k^{-5/2}$.

## 5. Discussion and conclusions

The dependence of the dynamics of rotating turbulence on the nature of the large-scale mechanical force is studied by means of numerical simulations to shed

light on the disparate results in the literature. For moderate Reynolds and low Rossby number flows we systematically vary the memory time scale $\tau_m$ of the mechanical force. As $\tau_m$ increases the forcing mechanism becomes less time-dependent and essentially less isotropic. We are able to demonstrate that different steady-state solutions will be reached if one is able to integrate for long enough time scales, showing the dependence of the flows on the forcing mechanism. When $\tau_m \propto \tau_{NL}$ we observe that mirror-symmetry spontaneously breaks in the flow even though our mechanical force is non-helical. Moreover, as the forcing mechanism becomes less time-dependent (long $\tau_m$) the net helicity increases. This is also true for the highest Reynolds number simulations that we carried out. We notice that helical waves break the tendency of the small and intermediate scales of the flows with the time-independent forcing to become 2D due to the imposed strong rotation. This makes the flow less anisotropic in contrast with a flow with highly random-in-time forcing where the net helicity appears to be negligible.

In addition, for moderate $Re_f$ and low $Ro_f$ flows both the power laws for the energy spectrum and the forward and inverse fluxes of energy depend strongly on the forcing mechanism. Depending on the value of $\tau_m$ we obtain different scaling of the energy spectrum with $E(k) \propto k^{-5/3}$, $k^{-2}$ and $k^{-5/2}$ showing a clear dependence of the spectral dynamics on the nature of the external driving force. Alexakis (2015) showed that no matter how large the Reynolds number can be there is a small enough Rossby number such that the flow exhibits a particular behaviour (e.g. weakly rotating turbulence, quasi-2D condensates) provided that an appropriate $\alpha > 0$ is considered in the scaling $Ro_f \propto Re_f^{-\alpha}$ (where $\alpha$ is expected to depend on the external driving force). So, lack of universality seems plausible in forced rotating turbulent flows. To corroborate this argument a large extent of the control parameter space should be covered with higher Reynolds number and lower Rossby number simulations integrated for extremely long times. However, this is beyond the reach of current computational capabilities.

The Rossby number dependence on the dynamics of flows with a highly random-in-time and time-independent mechanical force is also investigated at moderate Reynolds numbers. For weakly rotating turbulence (high $Ro_f$) the total energies of the two systems are comparable. Even so, for small enough $Ro_f$, even though large-scale vortices are present in both systems, energy condensates at large scales only for the flow with the time-independent forcing, as the energy spectra demonstrate.

Moreover, for large $Ro_f$ the net helicities of the two systems are zero but as $Ro_f$ becomes smaller there is a critical $Ro_f^{crit}$ at which the flow with the time-independent forcing bifurcates discontinuously from a non-helical state to a helical state. On the other hand, the helicity of the flow with the random-in-time forcing remains zero for all values of $Ro_f$. Based on this observation we argue that the angle between $\Omega \boldsymbol{e}_z$ and $\boldsymbol{\nabla} \times \boldsymbol{f}$ is important for the excitation of the inertial waves and consequently for the generation of net helicity in rotating flows. Thus, a time-independent forcing adds a preferred direction of propagation to the inertial waves inducing the mirror-symmetry breaking in our flows, since this angle is fixed in time. From the other side, a highly random-in-time forcing can excite inertial waves in all directions in equal proportions, and this is why the net helicity remains zero for any value of $Ro_f$. Such a mechanism has also been proposed for planetary dynamos (Moffatt 1970).

In the end, the lack of consistency of the results in the literature is attributed here to the forcing-dependent dynamics of forced rotating turbulent flows. Experiments should be able to show if this is true at higher Reynolds and lower Rossby numbers. The spontaneous emergence of helicity in such flows is an important aspect with

implications for cyclone persistence and intensity in supercell thunderstorms, a phenomenon that defies weather forecasting (Markowski *et al.* 1998), and also for planetary dynamos.

**Acknowledgements**

V.D. would like to thank A. Alexakis for enlightening discussions on rotating Taylor–Green flows. V.D. would also like to thank A. Alexakis and M. Linkmann for their useful comments on the first draft of the manuscript. V.D. acknowledges support from the Royal Society and the British Academy of Sciences (Newton International Fellowship, NF140631). The computations were performed on ARC1 and ARC2, part of the High Performance Computing facilities at the University of Leeds, UK.

## REFERENCES

ALEXAKIS, A. 2015 Rotating Taylor–Green flow. *J. Fluid Mech.* **769**, 46–78.

ANDRÉ, J. C. & LESIEUR, M. 1977 Influence of helicity on the evolution of isotropic turbulence at high Reynolds number. *J. Fluid Mech.* **81**, 187–207.

BARTELLO, P., MÉTAIS, O. & LESIEUR, M. 1994 Coherent structures in rotating three-dimensional turbulence. *J. Fluid Mech.* **273**, 1–29.

BEWLEY, G. P., LATHROP, D. P., MAAS, L. R. M. & SREENIVASAN, K. R. 2007 Inertial waves in rotating grid turbulence. *Phys. Fluids* **19**, 071701.

BOFFETTA, G. & ECKE, R. E. 2012 Two-dimensional turbulence. *Annu. Rev. Fluid Mech.* **44** (1), 427–451.

VAN BOKHOVEN, L. J. A., CLERCX, H. J. H., VAN HEIJST, G. J. F. & TRIELING, R. R. 2009 Experiments on rapidly rotating turbulent flows. *Phys. Fluids* **21**, 096601.

BRACCO, A. & MCWILLIAMS, J. C. 2010 Reynolds-number dependency in homogeneous, stationary two-dimensional turbulence. *J. Fluid Mech.* **646**, 517–526.

CAMBON, C., MANSOUR, N. N. & GODEFERD, F. S. 1997 Energy transfer in rotating turbulence. *J. Fluid Mech.* **337**, 303–332.

CONSTANTIN, P. & MAJDA, A. 1988 The Beltrami spectrum for incompressible fluid flows. *Commun. Math. Phys.* **115**, 435–456.

DALLAS, V. & ALEXAKIS, A. 2015 Self-organisation and non-linear dynamics in driven magnetohydrodynamic turbulent flows. *Phys. Fluids* **27**, 045105.

DALLAS, V., FAUVE, S. & ALEXAKIS, A. 2015 Statistical equilibria of large scales in dissipative hydrodynamic turbulence. *Phys. Rev. Lett.* **115**, 204501.

DAVIDSON, P. A., STAPLEHURST, P. J. & DALZIEL, S. B. 2006 On the evolution of eddies in a rapidly rotating system. *J. Fluid Mech.* **557**, 135–144.

DEUSEBIO, E., BOFFETTA, G., LINDBORG, E. & MUSACCHIO, S. 2014 Dimensional transition in rotating turbulence. *Phys. Rev.* E **90**, 023005.

DOMBRE, T., FRISCH, U., GREENE, J. M., HNON, M., MEHR, A. & SOWARD, A. M. 1986 Chaotic streamlines in the abc flows. *J. Fluid Mech.* **167**, 353–391.

GALTIER, S. 2003 Weak inertial-wave turbulence theory. *Phys. Rev.* E **68**, 015301.

GÓMEZ, D. O., MININNI, P. D. & DMITRUK, P. 2005 Parallel simulations in turbulent MHD. *Phys. Scr.* **T116**, 123–127.

GREENSPAN, H. P. 1968 *The Theory of Rotating Fluids*. Cambridge University Press.

HIDE, R. 1975 A note on helicity. *Geophys. Fluid Dyn.* **7** (1), 157–161.

HOPFINGER, E. J. & HEIJST, G. J. F. V. 1993 Vortices in rotating fluids. *Annu. Rev. Fluid Mech.* **25**, 241–289.

HOSSAIN, M. 1994 Reduction in the dimensionality of turbulence due to a strong rotation. *Phys. Fluids* **6**, 1077–1080.

KOLMOGOROV, A. N. 1941 The local structure of turbulence in incompressible viscous fluid for very large Reynolds number. *Dokl. Akad. Nauk SSSR* **30**, 301–305.

LIGHTHILL, J. 1965 *Waves in Fluids*. Cambridge University Press.

MALTRUD, M. E. & VALLIS, G. K. 1991 Energy spectra and coherent structures in forced two-dimensional and beta-plane turbulence. *J. Fluid Mech.* **228**, 321–342.

MARINO, R., MININNI, P. D., ROSENBERG, D. & POUQUET, A. 2013 Emergence of helicity in rotating stratified turbulence. *Phys. Rev.* E **87**, 033016.

MARKOWSKI, P. M., STRAKA, J. M., RASMUSSEN, E. N. & BLANCHARD, D. O. 1998 Variability of storm-relative helicity during VORTEX. *Mon. Weath. Rev.* **126** (11), 2959–2971.

MININNI, P. D., ALEXAKIS, A. & POUQUET, A. 2009 Scale interactions and scaling laws in rotating flows at moderate Rossby numbers and large Reynolds numbers. *Phys. Fluids* **21**, 015108.

MININNI, P. D. & POUQUET, A. 2009 Helicity cascades in rotating turbulence. *Phys. Rev.* E **79**, 026304.

MININNI, P. D. & POUQUET, A. 2010 Rotating helical turbulence. I: global evolution and spectral behavior. *Phys. Fluids* **22**, 035105.

MININNI, P. D., ROSENBERG, D. & POUQUET, A. 2012 Isotropization at small scales of rotating helically driven turbulence. *J. Fluid Mech.* **699**, 263–279.

MOFFATT, H. K. 1970 Dynamo action associated with random inertial waves in a rotating conducting fluid. *J. Fluid Mech.* **44**, 705–719.

MOFFATT, H. K. 1978 *Magnetic Field Generation in Electrically Conducting Fluids*. Cambridge University Press.

MOISY, F., MORIZE, C., RABAUD, M. & SOMMERIA, J. 2011 Decay laws, anisotropy and cyclone – anticyclone asymmetry in decaying rotating turbulence. *J. Fluid Mech.* **666**, 5–35.

MORINISHI, Y., NAKABAYASHI, K. & REN, S. 2001 Effects of helicity and system rotation on decaying homogeneous turbulence. *JSME Intl J.* B **44**, 410–418.

POUQUET, A. & MININNI, P. D. 2010 The interplay between helicity and rotation in turbulence: implications for scaling laws and small-scale dynamics. *Phil. Trans. R. Soc. Lond.* A **368** (1916), 1635–1662.

POUQUET, A., SEN, A., ROSENBERG, D., MININNI, P. D. & BAERENZUNG, J. 2013 Inverse cascades in turbulence and the case of rotating flows. *Phys. Scr.* T **155**, 014032.

PROUDMAN, J. 1916 On the motion of solids in a liquid possessing vorticity. *Proc. R. Soc. Lond.* A **92** (642), 408–424.

RUPPERT-FELSOT, J. E., PRAUD, O., SHARON, E. & SWINNEY, H. L. 2005 Extraction of coherent structures in a rotating turbulent flow experiment. *Phys. Rev.* E **72**, 016311.

SEN, A., MININNI, P. D., ROSENBERG, D. & POUQUET, A. 2012 Anisotropy and nonuniversality in scaling laws of the large-scale energy spectrum in rotating turbulence. *Phys. Rev.* E **86**, 036319.

SMITH, L. M., CHASNOV, J. R. & WALEFFE, F. 1996 Crossover from two- to three-dimensional turbulence. *Phys. Rev. Lett.* **77**, 2467–2470.

TAYLOR, G. I. 1917 Motion of solids in fluids when the flow is not irrotational. *Proc. R. Soc. Lond.* A **93** (648), 99–113.

TEITELBAUM, T. & MININNI, P. D. 2011 The decay of turbulence in rotating flows. *Phys. Fluids* **23** (6), 065105.

TOBIAS, S. M. 2009 The solar dynamo: the role of penetration, rotation and shear on convective dynamos. *Space Sci. Rev.* **144**, 77–86.

TRITTON, D. J. 1988 *Physical Fluid Dynamics*. Clarendon Press.

WALEFFE, F. 1992 The nature of triad interactions in homogeneous turbulence. *Phys. Fluids* A **4** (2), 350–363.

YEUNG, P. K. & ZHOU, Y. 1998 Numerical study of rotating turbulence with external forcing. *Phys. Fluids* **10**, 2895–2909.

YOSHIMATSU, K., MIDORIKAWA, M. & KANEDA, Y. 2011 Columnar eddy formation in freely decaying homogeneous rotating turbulence. *J. Fluid Mech.* **677**, 154–178.

ZHOU, Y. 1995 A phenomenological treatment of rotating turbulence. *Phys. Fluids* **7** (8), 2092–2094.